Notice

Manuscript details

Title: Kathmandu Basin as a local modulator of seismic waves: 2D modelling of nonlinear site response under obliquely incident waves

Authors: Elif ORAL (Geoazur/CalTech), Peyman AYOUBI (CalTech), Jean-Paul Ampuero (Geoazur), Domniki Asimaki (CalTech), Luis Fabian Bonilla (IFSTTAR)

Contact: elifo@caltech.edu

submitted to *Geophys. J. Int.*

Kathmandu Basin as a local modulator of seismic waves: 2D modelling of nonlinear site response under obliquely incident waves

Elif Oral[1,2], Peyman Ayoubi[2], Jean Paul Ampuero[1], Domniki Asimaki[2], Luis Fabian Bonilla[3]

[1] *Université Côte d'Azur, IRD, CNRS, Observatoire de la Côte d'Azur, Géoazur, 06560 Valbonne, France*

[2] *Mechanical and Civil Engineering, California Institute of Technology, Pasadena CA 91125, USA*

[3] *Geotechnical Engineering, Environment, Natural hazards and Earth sciences Department, Université Gustave Eiffel, 77447 Marne-la-Vallée Cedex 2, France*

10 October 2021

SUMMARY

The 2015 M_w 7.8 Gorkha, Nepal earthquake is the largest event to have struck the capital city of Kathmandu in recent times. One of its surprising features was the frequency content of the recorded ground motion, exhibiting a notable amplification at low frequencies (< 2 Hz) and a contrasting depletion at higher frequencies. The latter has been partially attributed to the damper behaviour of the Kathmandu basin. While such weak high-frequency ground motion helped avoiding severe damage in the city, the catastrophic outcomes of earlier earthquakes in the region attest to a contrasting role of the Kathmandu basin as a broadband amplifier, in addition to possible source effects. Given the possibility of future strong events in the region, our main objective is to elucidate the seismic behaviour of the Kathmandu basin by focusing on site effects. We numerically model 2D P-SV wave propagation in a broad frequency band (up to 10 Hz), incorporating the most recent data for the Kathmandu basin geometry, soil stratigraphy and geotechnical soil properties, and accounting for the non-linear effect of multi-dimensional soil plasticity on wave propagation. We find that: 1) the Kathmandu basin generally amplifies low frequency ground motion

(< 2 Hz); 2) waves with large incidence angles relative to vertical can dramatically amplify the high frequency ground motion with respect to bedrock despite the damping effect of soil nonlinearity; 3) the spatial distribution of peak ground motion amplitudes along the basin is highly sensitive to soil nonlinearity and wave incidence (angle and direction), favoring larger values near the basin edges located closer to the source, as observed during the 2015 event. Our modelling approach and findings can support the ongoing resilience practices in Nepal and can guide future seismic hazard assessment studies for other sites that feature similar complexities in basin geometry, soil stratigraphy and dynamic soil behaviour.

Key words: Numerical modelling, Earthquake ground motions, Site effects, Wave propagation, Elasticity and anelasticity, Asia

1 INTRODUCTION

The 25 April 2015 Gorkha, Nepal earthquake (magnitude 7.8) was the largest event to hit the capital city of Kathmandu in recent times, yet seismic hazard in the region remains high (e.g., Avouac et al. 2015; Galetzka et al. 2015; Rajaure et al. 2017). The rupture broke the bottom portion of the locked zone of an eastern segment of the Main Himalayan Thrust (MHT) (Avouac et al. 2015; Zhang et al. 2016). Kathmandu is located within 80 km of the epicenter. Within a month, two M6+ aftershocks occurred (magnitudes 6.7 and 6.8) in the southeast of the mainshock epicenter. The following day, the strongest aftershock of magnitude 7.3 occurred east of Kathmandu, near Dolakha, and was followed by a M 6.2 aftershock in its proximity (Fig. 1a). The ruptures during this sequence of five events did not reach to shallower parts of the fault. The possibility of stress transfer to the unbroken shallower portion of the fault and the long-known seismic gap in the western part of the MHT underline the likelihood of another M7+ megathrust event in the area (Avouac et al. 2015; Dal Zilio et al. 2019).

The seismic response of the Kathmandu basin during the Gorkha event was particular: ground motion was notably weak at high frequencies and enhanced at low frequencies compared to empirical expectations (e.g., Galetzka et al. 2015; Rajaure et al. 2017; Takai et al. 2016; Asimaki et al. 2017). The recorded amplitudes at the stations of the Kathmandu Valley were below the estimations of ground motion prediction equations (GMPE) at frequencies

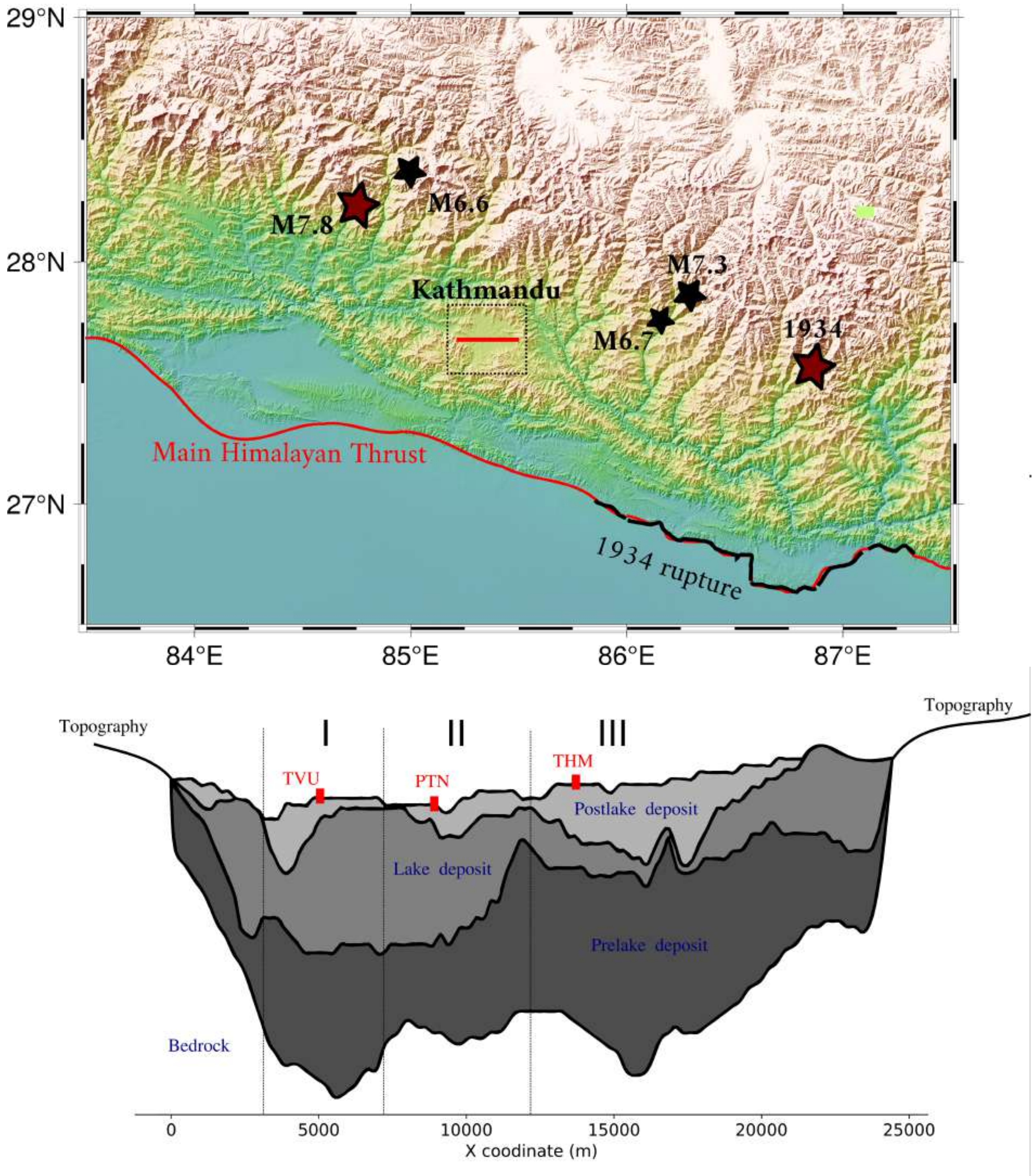

Figure 1. Overview of the 2015 Gorkha, Nepal earthquake sequence and Kathmandu basin. (Top) Epicentres of the selected past earthquakes (stars), surface trace of the Main Himalayan Thrust (red curve), lateral extension of the 1934 rupture (black curve), and location of the Kathmandu basin (black dashed square, with the red line indicating the 2D cross-section). (Bottom) Detailed view of the 2D basin model, with vertical axis scaled 10 times for better visualisation. Red squares indicate the locations of seismic stations.

higher than about 2 Hz (Rajaure et al. 2017; Hough et al. 2016). Since such weakness of high-frequency ground motion was observed at both rock and soil stations, it is mainly associated with source effects, namely a deficiency of high-frequency radiation by the earthquake rupture in the proximity of the basin. Soil nonlinearity is an additional factor that could have led to further attenuation of high-frequency ground motion inside the basin, and is a subject of the present work. Ground motion amplification by the basin, quantified by peaks in the basin-to-rock spectral ratios of ground motion, was observed to occur at lower frequencies during the strongest events of the sequence (M 7.8 Gorkha mainshock and M 7.3 Dolakha aftershock) than during the weaker aftershocks. This observation was interpreted as a reduction of the resonance frequency of the basin induced by soil nonlinearity (e.g., Rajaure et al. 2017; Asimaki et al. 2017).

On the other hand, low-frequency ground motion in Kathmandu was enhanced due to site effects controlled by the basin geometry and soil stratigraphy. A striking difference between the recordings of rock and soil stations is the prolonged ground motion at the soil stations at low frequencies, on the order of 40 seconds longer. This difference is exemplified in Figure 2 by comparing the recordings of a rock station (KTP) and a soil station (TVU) that are separated by less than 1 km — short enough to ignore differences in source effects. Moreover, during all the events of the Gorkha sequence, the ground motion Fourier spectra below $\sim$ 2 Hz at soil stations were up to 5 times larger than at rock stations, which is an indication of site effects of the Kathmandu basin (e.g., Rajaure et al. 2017). The amplification of ground motion at low frequencies due to basin resonance is indeed a well-recognised phenomenon that has been reported for many areas, such as Seattle, USA (Frankel et al. 2002), L'Aquila, Italy (De Luca et al. 2005), and Quito, Ecuador (Laurendeau et al. 2017).

Concerning high-frequency ground motion, Kathmandu basin may have played a contrasting role during past earthquakes. Prior to the 2015 earthquake, severe seismic vulnerability was reported for the structures in the Kathmandu Valley (JICA 2002; Dixit et al. 2013). The weakness of the high-frequency ground motion during the Gorkha sequence, which was partially due to the basin nonlinearity as discussed above, was a fortunate feature: it may have prevented further damages in Kathmandu. Damage was not severe on residential structures, which are

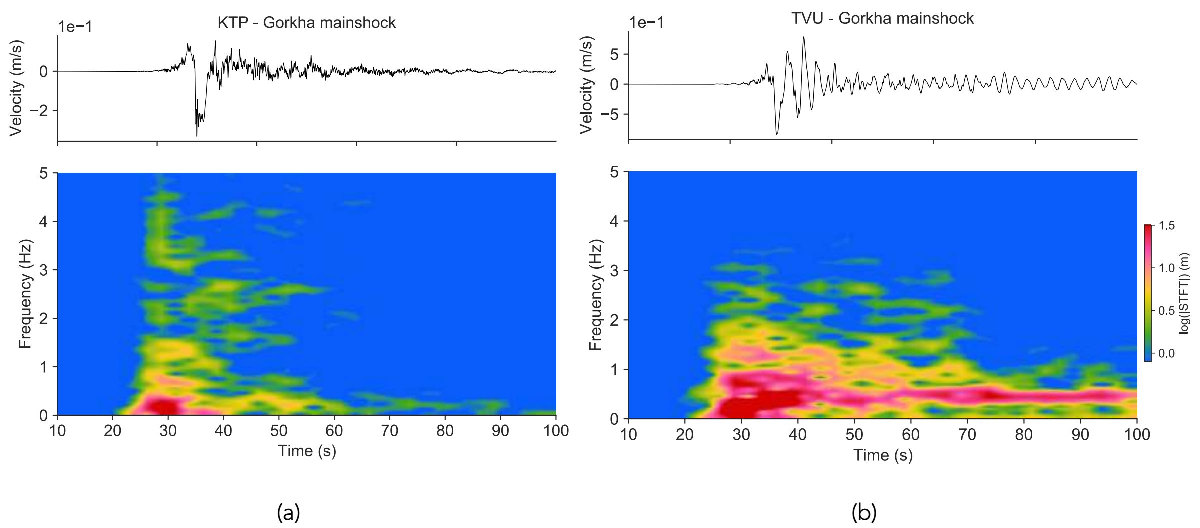

Figure 2. Ground motion recordings of the 2015 Gorkha earthquake at rock and soil stations. East-west ground velocity time histories (top) and short-time Fourier transform spectogram (bottom) for the rock station KTP (a) and the soil station TVU (b). Origin time is 2015-04-25 06:11:25.95.

commonly reinforced concrete buildings with masonry infills, mostly three to four stories high, and sensitive to higher frequencies than high-rise buildings (Chiaro et al. 2015; Hashash et al. 2015; Kaushik et al. 2016). By contrast, available documentation on earlier earthquakes points to extensive and much higher human and damage tolls (e.g., Sapkota et al. 2013; Dixit et al. 2013). For example, the 15 January 1934 earthquake, which likely had a magnitude of M_w 8.1-8.2, caused great destruction and 11,000 deaths (Auden & Ghosh 1935; Singh & Gupta 1980). Its extensive damage in Kathmandu was possibly due to strong amplification inside the basin (e.g., Hough & Roger 2008). Similar outcomes were also reported for the 1255 earthquake (e.g., Sapkota et al. 2013). In light of such a contrast between the impact of different earthquakes on Kathmandu, and given the poor construction practice (e.g., Dixit et al. 2013), we hypothesise a stronger high-frequency ground motion for the events before the Gorkha earthquake.

Given the high seismic hazard and the possible disparity of the Kathmandu basin behaviour in the past, we primarily address the following question: What seismic response of the Kathmandu basin should we expect during future earthquakes — possibly a different frequency content or spatial distribution than during the Gorkha earthquake? To answer this question, we here focus on site effects: despite possibly short source-to-site distance, we ignore complexities arising from fault finiteness by limiting our study to the assumption of plane wave incidence.

We numerically model the 2D broadband seismic response of the Kathmandu basin for linear and non-linear soil behaviour and different wave incidences. Previous numerical modelling of the Gorkha earthquake supported that the Kathmandu basin can enhance low frequency ground motion (Ayoubi et al. 2018; Wei et al. 2018) and attenuate high frequency ground motion by soil nonlinearity (Ayoubi et al. 2018; Chen & Wei 2019), but these studies were based on substantial simplifications, notably simplified basin geometry and soil stratigraphy, and 1D modeling of soil nonlinearity. Here we take these initial efforts a step further, by considering a realistic basin structure and geotechnical soil properties, obtained by a recent geotechnical survey (SAFER, Gilder et al. 2020), together with a 2D nonlinear modelling approach that couples 2D basin effects and multi-dimensional soil plasticity (Oral et al. 2019). Previous work showed that the amplification of ground motion due to basin effects can be severely damped by soil nonlinearity (Marsh et al. 1995; Psarropoulos et al. 2007; Roten et al. 2014; Esmaeilzadeh et al. 2019), yet a 1D wave propagation modelling approach underestimates the ground motion even when soil nonlinearity is triggered (Ragozzino 2014; Chen et al. 2015; Oral et al. 2019). Moreover, 2D and 3D wave propagation effects also enhance nonlinearity when multi-dimensional soil plasticity is considered, compared to 1D plasticity, which can affect final surface displacement (e.g., Oral et al. 2017). Thus the consideration of multi-dimensional soil plasticity is necessary for a robust estimation of ground motion amplitudes. In addition, as reported in earlier studies on simplified 2D basin models, wave incidence angle can significantly impact the amplitude, duration and spatial distribution of ground motion (Liu et al. 1991; Papageorgiou & Kim 1993; Bonilla et al. 2011; Zhu et al. 2016; Zhang et al. 2017). Site-specific features, such as surface topography, irregular geometry of layer interfaces, and asymmetry of basin geometry, can further contribute to variability of ground motion across the basin (e.g., Ragozzino 2014) and are not well captured by 1D modelling approaches. Given that the Kathmandu basin is surrounded by active faults and is not symmetrical, we also investigated the sensitivity of the ground motion inside the Kathmandu basin to the obliquity of incident waves.

In the following, we first present the studied area, and the methods and data used for numerical modelling. Then, we report our results on site effects in the Kathmandu basin at low and high frequencies. Next, we discuss the spatial variation of ground motion along the Kathmandu basin. Last, we summarise our main findings and perspectives for future research.

2 METHODS AND SITE PROPERTIES

Kathmandu is located on an intermontane basin in the midland of the Lesser Himalayas (Sakai et al. 2002). Here we study one of its 2D cross-sections that extends in the east-west direction. We first created the 3D geometry of the Kathmandu basin by combining the sub-surface images of Piya (2004) with geotechnical data. Piya (2004) developed a database of subsurface geometry for liquefaction hazard assessment; we processed these images with the geotechnical dataset of SAFER (Gilder et al. 2020) and obtained a 3D model of the basin geometry. For the numerical models in this study, we selected a 2D cross-section that covers the locations of the stations that were deployed by Takai et al. (2016), as indicated by the red line in Fig. 1a.

We set three sediment layers for the basin and consider that the shallowest layer is nonlinear. Figure 1b displays the geometry of the layers in our 2D section. The deepest part is mostly filled with sand and gravel; the middle part is mainly clay; and the shallowest part is made of fine-to-medium sand, and silt intercalated with clays (Sakai 2001). Outside the basin, basement rock is formed by Precambrian to Devonian rocks. In accordance with this knowledge, we set three types of basin soil: Bagmati (prelake deposit), Kalimati (lake deposit) and Patan (postlake deposit). The basin model has a length of 24.4 km and a maximum depth of about 450 m in the central part. We referred to the recent geotechnical project SAFER (Gilder et al. 2020) while setting up the soil properties in the 2D Kathmandu basin model, listed in Table 1. To simplify the evaluation in the following, we virtually divided the basin into three sections, referred to hereafter as the western, middle, and eastern parts of the basin, respectively, as denoted by I, II, and III in Fig. 1b.

In the absence of detailed knowledge of soil nonlinearity properties, we assumed that only the first layer is nonlinear, given its soil type, relatively shallow depth and low velocity. We set a cohesion and friction angle of 20 kPa and 10 degree, respectively. We verified our choice by determining soil nonlinearity properties, mainly the backbone curve, from the shift of resonance frequencies observed during strong events, by applying the method of Castro-Cruz et al. (2020)

Table 1. Soil properties of the Kathmandu basin model.

Layer	Soil type	Density	V_p (m/s)	V_s (m/s)	Q_p	Q_s
Postlake deposit	Fine to medium sand and silt	1600	416.33	200	40	20
Lake deposit	Clay	1800	810.00	425	80	40
Prelake deposit	Gravel and Sand	2000	2298.40	1250	230	125
Bedrock	Precambrian to Devonian rocks	2530	5500.00	3200	300	150

to the ground motion recordings of the Gorkha sequence (detailed in SI). In our models, the overburden (or effective) stress increases with depth, such that the backbone curve varies with depth inside the nonlinear layer. With our choice of nonlinearity parameters, the mid-layer has a backbone curve consistent with the one obtained by frequency-shift analysis. In addition, for all layers, we considered viscoelastic attenuation by setting quality factors that approximately equal 10% of the velocity values, as shown in the table. We denote the viscoelastic cases as 'linear' cases throughout the manuscript.

We numerically modelled seismic wave propagation in linear and nonlinear media in 2D with P-SV polarisation (in-plane). We used the spectral element method (e.g. Komatitsch & Vilotte 1998; Chaljub et al. 2007) implemented in the software SEM2DPACK for 2D seismic wave propagation (Ampuero et al. 2002; Ampuero 2012) including soil nonlinearity (Oral et al. 2019). (See Data and resources section for software availability.) The implemented model of soil nonlinearity follows the Iwan (1967) method and is based on the formulation of Joyner (1975), as detailed in Oral et al. (2019). We set the element size to achieve a good resolution of the wavefield up to 10 Hz, accounting for possible velocity reduction due to soil nonlinearity. We set the boundary conditions as periodic on the sides, free surface on top, and absorbing (Clayton & Engquist 1977) at the bottom. We verified for both vertical and oblique incidence cases that our model set-up satisfactorily works to avoid artificial reflections from boundaries towards the basin. We use the leap-frog scheme for time discretisation and set the time step to satisfy a Courant-Friedrichs-Lewy (CFL) condition with Courant number ≤ 0.3.

We analysed different levels of triggered soil nonlinearity by comparing the basin response to two different input motions with same amplitude but contrasting waveform complexity. Triggered soil nonlinearity is known to correlate with the peak amplitude of input motion: a dynamic

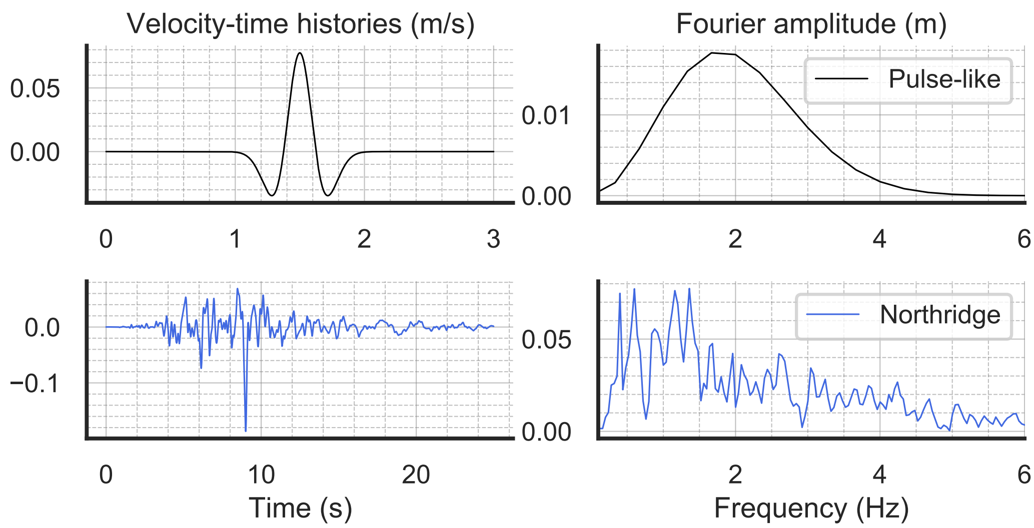

Figure 3. Input motions used in the simulations. Velocity-time histories (left) and Fourier amplitude (right) for the pulse-like input (top) and the Northridge input (bottom).

loading with a larger peak acceleration generally induces larger plastic strain. In addition, the complexity of the input motion, qualified by the number of loading-unloading cycles, also affects the level of soil nonlinearity (Gélis & Bonilla 2012). This implies that stronger nonlinearity can be expected for input time histories with more zero-crossings. Thus, we prepared two input motions, with the same peak acceleration of 0.1 g —simply by scaling their amplitude— but contrasting level of complexity: a smooth pulse-like input motion made of a Ricker wavelet (hereafter referred to as ‘pulse-like’ input) and a real input motion based on the recording of the 1994 Northridge earthquake at LA00 station in the east-west direction (hereafter referred to as ‘Northridge’ input). Figure 3 displays their velocity-time histories and corresponding Fourier amplitudes. Both inputs have sufficiently high energy below 5 Hz, and the Northridge spectrum peaks at half lower frequency ($\sim$ 1 Hz) than the pulse-like spectrum.

3 RESULTS

3.1 Kathmandu Basin typically enhances the low-frequency ground motion (< 2 Hz)

We find that the Kathmandu Basin can amplify low-frequency ground motion with and without soil nonlinearity. Figure 4a displays the site-to-rock spectral ratios along the basin length for linear and nonlinear models up to 4 Hz, the upper frequency at which the input motions have substantial energy (Fig. 3). We used the geometric mean of the fast Fourier amplitudes of ground motion at rock stations when calculating the spectral ratios. To isolate the effect of rheology, we considered vertically incident plane waves. In the linear model, the spectral ratios reach values around 8 inside the basin, in particular below 2 Hz. We find fundamental frequencies in the range of 0.3-1.5 Hz. The largest spectral ratios correspond to about 0.5 Hz mostly in the central basin sections. Spatial variations to higher values are present near local basin edges as expected given the irregularities of the basin geometry and layer interfaces, and the rough topography near the basin edges (Fig. 1b). Our frequency range is in agreement with the 0.1-2.5 Hz range reported in the observational studies on the Gorkha earthquake cited above. Potential reasons for the narrower range found here are the lack of 3D effects (coupling of P-SV and SH waves), geometrical features at surface and depth that are not represented in our 2D cross-section, and a spatial variability of the presence of nonlinear layers and triggered nonlinearity in contrast to our assumption that only the 1st layer is nonlinear. Investigating whether the inclusion of these factors can capture the reported frequency range of basin resonance is of interest for further studies on Kathmandu. Consideration of basin nonlinearity notably reduces the spectral ratios for both input motions. However, the spectral amplification around the fundamental frequency persists. Thus, the Kathmandu Basin can enhance low-frequency ground motion, as observed during the Gorkha earthquake, for both linear and nonlinear basin rheologies.

Pronounced low-frequency ground motion in the Kathmandu Basin also occurs under oblique wave incidence. In Figure 5, we present the soil-to-rock spectral ratios for three wave incidence angles relative to the vertical axis: 30 degrees from west, 0 degrees and 30 degrees from east. An incidence of 30 degrees is plausible for the regional seismotectonics and useful for comparison purposes. We used the Northridge input and considered soil nonlinearity in all the three cases. The change of incidence angle causes local variations in the fundamental frequencies and spatial pattern of the spectral ratios. If incidence is from west (east), the largest amplification appears in the western (eastern) side of the basin. In all cases, the largest soil-to-rock spectral ratios occur at low frequencies, below 2 Hz, which corroborates the amplification of low frequency ground motion by the Kathmandu basin effects.

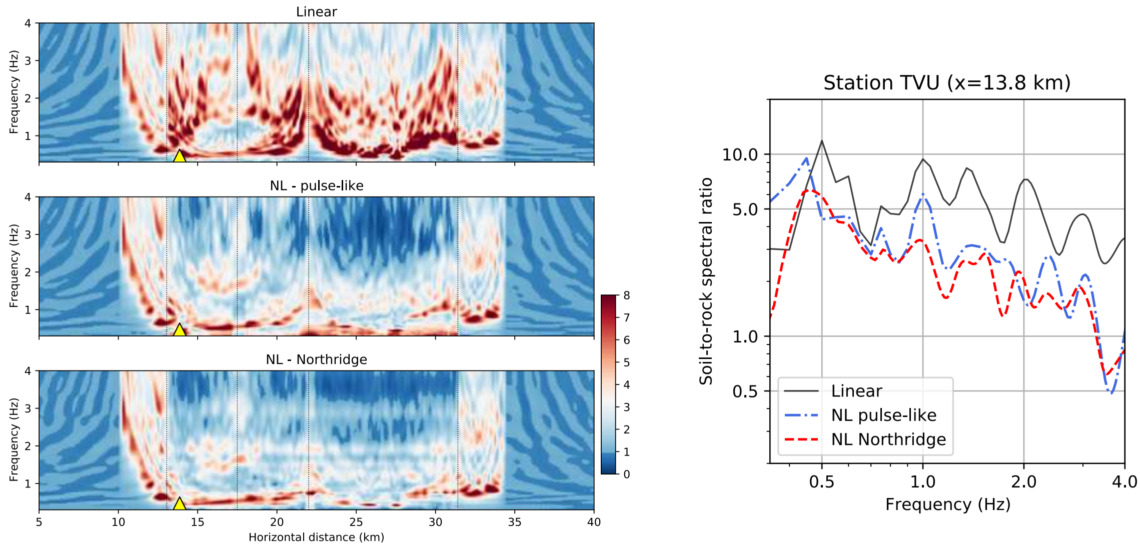

Figure 4. Site-to-rock spectral ratios for different soil rheologies. (Left) 2D spectral ratios for a viscoelastic model (top) and nonlinear models with pulse-like input (middle) and Northridge input (bottom). (Right) Spectral ratios of the three models at the location of station TVU (yellow triangle on the left plots). Wave incidence is vertical in the three cases. Outer and inner dashed lines indicate the basin-bedrock limits and inner basin sections, respectively.

3.2 Oblique wave incidence can boost high frequency ground motion despite soil nonlinearity

Soil nonlinearity causes ground motion damping and local reduction of fundamental frequencies for the input motions used here. To evaluate how the soil nonlinearity can affect the wave propagation in the basin, we evaluated the soil-to-rock spectral ratios of the nonlinear cases with pulse-like and Northridge inputs (Figure 4). Both cases lead to smaller spectral ratios and slight reductions of fundamental frequencies compared to the linear simulation. As expected from the discussion in Section 2, the Northridge input case produces stronger nonlinearity than the pulse-like case, manifested by slightly smaller fundamental frequencies at certain basin locations (e.g., between 17 and 20 km) and additional damping that changes the spatial pattern of spectral ratios. The spectral ratios at the TVU station (Figure 4b) show a damping in both nonlinear cases up to a factor of 3 with respect to the linear case. The higher nonlinearity level in the Northridge case is seen at TVU by slightly smaller spectral ratios above $\sim$1 Hz. In addition, both nonlinear cases produce a slight shift in the resonance frequencies (from 0.5 Hz

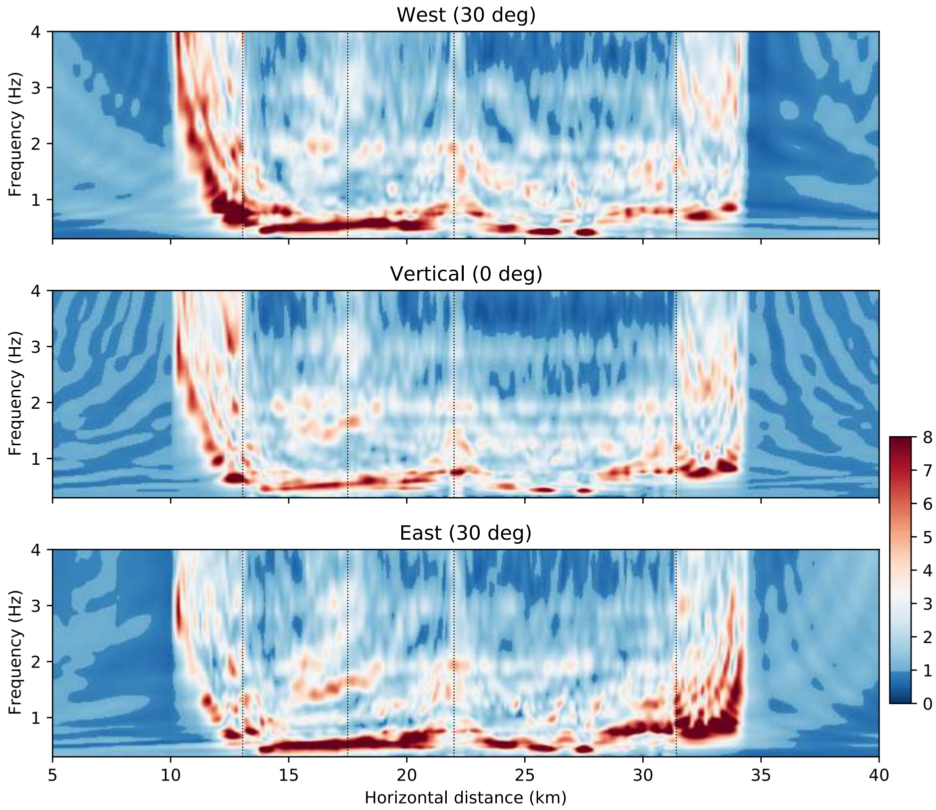

Figure 5. Site-to-rock spectral ratios for different cases of wave incidence. Shown for oblique incidence from west with 30 degrees (top), vertical incidence (middle), and oblique incidence from east with 30 degrees (bottom). We used Northridge input and considered soil nonlinearity in all the three cases. Outer and inner dashed lines indicate the basin limits and inner basin sections, respectively.

to 0.45 Hz for TVU), which are comparable to the reported frequency shift values during the Gorkha mainshock with respect to aftershocks.

Our further comparisons between the simulations using Gorkha and Northridge inputs support the role of source frequency-content on depletion of high frequency ground motion during the Gorkha earthquake, in addition to soil nonlinearity. We performed additional simulations by using as incident input motion the east-west component of the Gorkha event recording at the rock-site station KTP. For both the Gorkha and Northridge inputs, we first quantify the damping due to soil nonlinearity, specifically by calculating the relative change of Fourier spectrum integral of nonlinear case with respect to that of the linear case. Details about the chosen time windows to compute the damping percentages are given in SI. Figure 6 (a-b) shows the ground velocity Fourier amplitudes at the soil station TVU. For both input motions, soil nonlinearity causes notable reduction of the ground-motion spectral amplitude above 0.4 Hz, reaching more than 50% reduction relative to the linear case. Second, we quantified the difference of high frequency source content (above 0.4 Hz) between the two cases. In Figure 6c, we compare the spectra of the two input motions: The spectral content above 0.4 Hz in the Gorkha case is weaker by roughly 20 % compared to the Northridge case. In reality, incident ground motion can further vary due to the fault finiteness. Despite the plane wave assumption here, such a 20% vs 50% partition of the roles of source and soil nonlinearity on the high-frequency ground motion depletion underlines the likelihood of the coupled effect of these two factors during the Gorkha earthquake.

On the other hand, despite basin nonlinearity, a critically oblique wave incidence can boost the high frequency ground motion (> 2 Hz) inside the Kathmandu basin with respect to the outer rock. We performed an additional set of simulations with gradually increased incidence angles and adopting the Northridge input. Figure 7a shows the soil-to-rock spectral ratios in linear simulations with wave incidence angles of 30, 40 and 45 degrees from East. The basin strongly amplifies ground motion over a broader frequency band at increasing incidence angle. At 40 degrees of incidence, the amplification above 1 Hz is concentrated at the edges of the three sections of the basin, and the soil-to-rock spectral ratio reaches a factor of $\sim$10 below 5 Hz. At 45 degrees of incidence, the amplification is dramatically larger all over the basin. The theoretical value of refraction due to impedance contrast (by Snell's law) ranges between 20 and 28 degrees for the 1D simplification of the soil strata. Our additional 2D simulations probing more incidence angles (supporting figures in SI) show that strong broadband amplification above 2 Hz occurs at incidences higher than $\sim$42 degrees. Figure 7b shows the same comparison but including soil nonlinearity. The soil nonlinearity attenuates the ground motion for all the cases of wave incidence angle. Despite that, the enhanced high-frequency amplification at increasing incidence angle prevails. Such a dominant amplification effect is also seen at the locations of two soil stations, TVU and THM (Figure 8): their spectral ratios are a factor of $\sim$ 5 larger at 45 degrees incidence than at 30 degrees incidence, at frequencies > 0.5 Hz.

We propose that the incidence angle effect may have contributed to the differences in the response of the Kathmandu basin during past earthquakes, in addition to possible differences

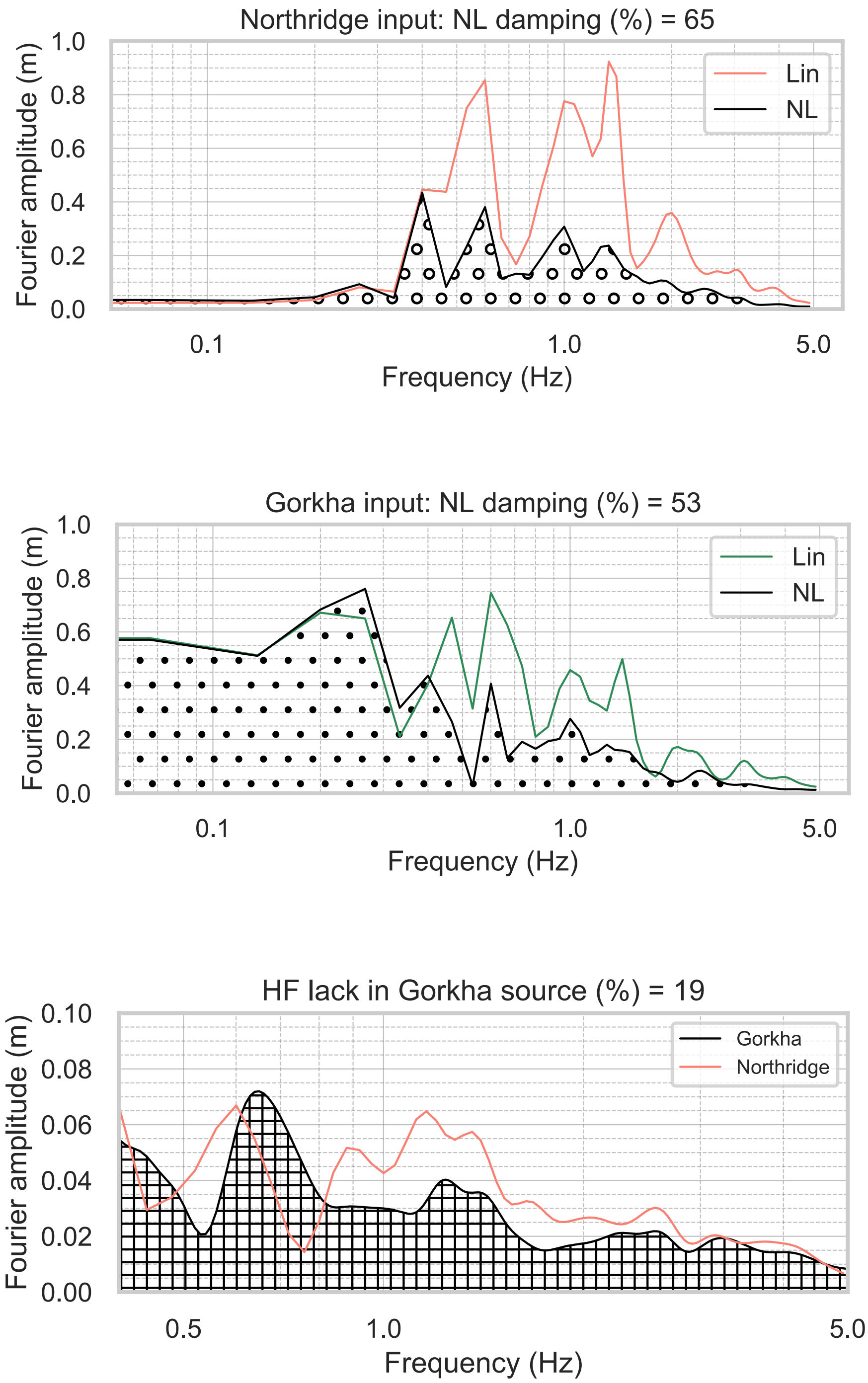

Figure 6. Quantification of high-frequency deficiency due to source and soil nonlinearity. Comparison of the Fourier amplitudes of basin ground motion between the elastic and nonlinear cases for the use of Northridge (top), and Gorkha (middle) input, and comparison of the Fourier amplitudes of Gorkha and Northridge input motions (bottom).

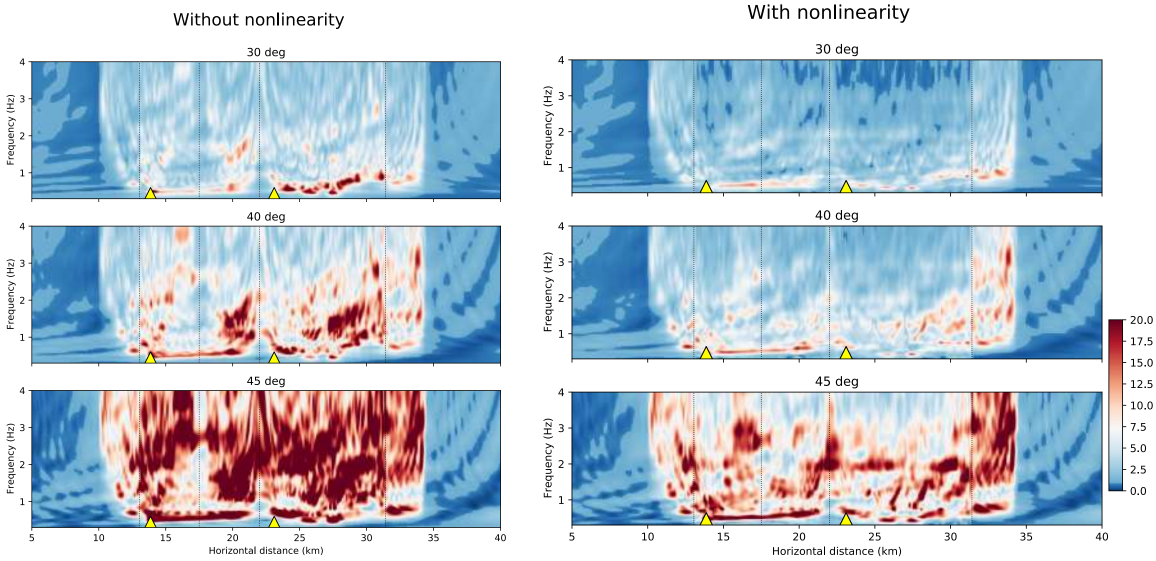

Figure 7. High-frequency ground motion amplification due to the criticality of wave incidence. Site-to-rock spectral ratios for oblique incidence with 30 degree (top), 40 degree (middle), and 45 degree (bottom), for linearity (left) and nonlinearity (right) considerations. Outer and inner dashed lines indicate the basin limits and inner basin sections, respectively. Locations of TVU (x=13.8 km) and THM (x=23.1 km) stations are denoted by triangles.

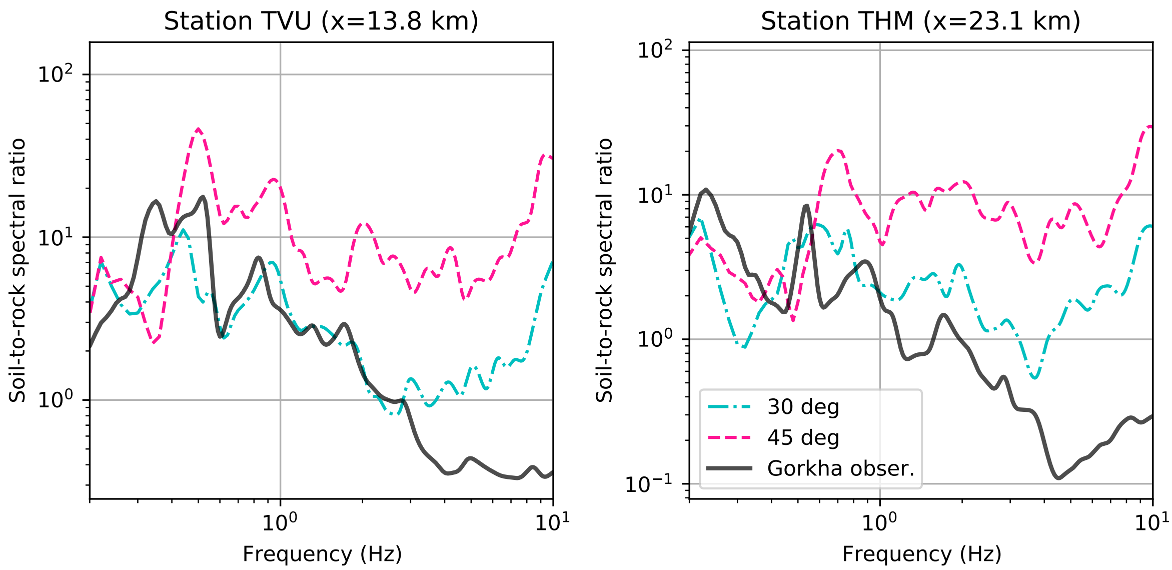

Figure 8. High-frequency ground motion amplification due to wave incidence angle at selected soil stations. Comparison of the soil-to-rock spectral ratios between the cases of 30 and 45 degrees, and the observation during the 2015 Gorkha earthquake, shown for stations TVU (left) and THM (right), calculated as the ratio of Fourier amplitudes between each station recording and that of KTP rock station.

of source frequency-content. The 2D cross-section that we are analysing extends almost parallel to the fault strike of the 2015 earthquake, in the east-west direction (Figure 1). Given that the rupture propagation was also in this direction during the 2015 earthquake, the real case scenario of the dominant incidence angle and direction is likely to have varied along our 2D model, differently than our plane wave assumption. Comparing our simulation results with the Gorkha observations, in Figure 8, the spectral ratios for the incidence of 30 degrees fit better the observations. At TVU station, there is good agreement up to frequencies of $\sim$2 Hz, and the resonance frequencies are mostly compatible. At THM station, the synthetics overestimate the observation, but the spectral shape is similar up to $\sim$4 Hz. Moreover, for both incidences the synthetic cases result in larger spectral ratios than the observations above $\sim$2 Hz. Because the Northridge input has a broader spectrum than the Gorkha source, this result supports the idea that a larger high-frequency amplification could have been observed if the Gorkha source had been richer in that frequency range. We do not have any means to make a similar evaluation for the earlier earthquakes (such as the 1255 and 1934 events) due to the absence of instrumentation at the time, which makes it unclear to assess whether these events are near- or far-field sources. Assuming near-field sources and given that those past earthquakes likely occurred farther from Kathmandu than the 2015 event and yet caused more damages in the Kathmandu basin, the incidence angle deserves to be accounted for in seismic hazard assessment studies for Kathmandu, besides possible source effects.

3.3 Soil nonlinearity and oblique wave incidence can sharpen the spatial heterogeneity of ground motion in the basin

The damping effect of soil nonlinearity in the Kathmandu basin enhances the contrast of peak ground motion amplitudes between the edges and deeper parts of the basin. We analysed the spatial variation of ground motion amplitudes across the basin and how it relates to the basin nonlinearity. Figure 9 displays the comparison of PGA along the basin length between linear and nonlinear cases, together with the maximum —total— strain reached in the nonlinear layer. Results are shown for the two input cases: pulse-like (top) and Northridge (bottom). Wave incidence is vertical in both cases. In the pulse-like input case, the shallower parts close to the basin edges undergo higher strains. In the Northridge input case, the maximum strain is higher everywhere. The stress-strain curves at locations close to eastern and western edges of the basin, Figure 9 (b, d), show higher complexity of the loading cycle for the Northridge input, consistently with its larger number of zero-crossings (See the discussion in 2). For both input motions, in the linear simulations, the PGA values are comparable all along the basin length, although the combined effects of basin geometry and soil stratigraphy lead to slightly larger PGA values close to corners and section boundaries (e.g., at x=13, 15, 18.5, 22, and 30 km). In the simulations with soil nonlinearity, PGA is strongly reduced everywhere there is a sufficiently thick nonlinear layer below but remains high elsewhere (details in SI). The local peaks in the deeper parts of the basin mostly disappear, and the PGA shows notable contrasts near the edges of basin sections favouring larger amplitudes where nonlinear soil is not thick. Despite higher level of nonlinearity triggered in such thin layers (e.g., x=22 km), the PGA in the proximity remains large, such that the PGA ratio between basin corners and deeper sections can rise to a factor of 5, as seen in the case of Northridge input (at x=22 km vs x=25 km).

The direction of wave incidence can cause further variation of triggered basin nonlinearity. Figure 10 compares the basin response to wave incidence from east and west, for the Northridge input. The incidence angle equals 30 degrees in both cases. Incidence from east results in larger strains in the eastern section. The effect of such higher nonlinearity on ground motion is rather slight, manifesting as further local variation of PGA in that section. Incidence from west triggers a similar effect on the western section.

Given that Kathmandu is inhabited by a dense population and hosting highly vulnerable constructions, our findings of the local variation of the ground motion due to the direction of wave incidence and soil nonlinearity warrant further research on regional seismic hazard including these factors. Our study is limited to plane wave incidence, and further investigation of the spatial variability of ground motion deserves a closer look into possible effects of source finiteness and rupture directivity.

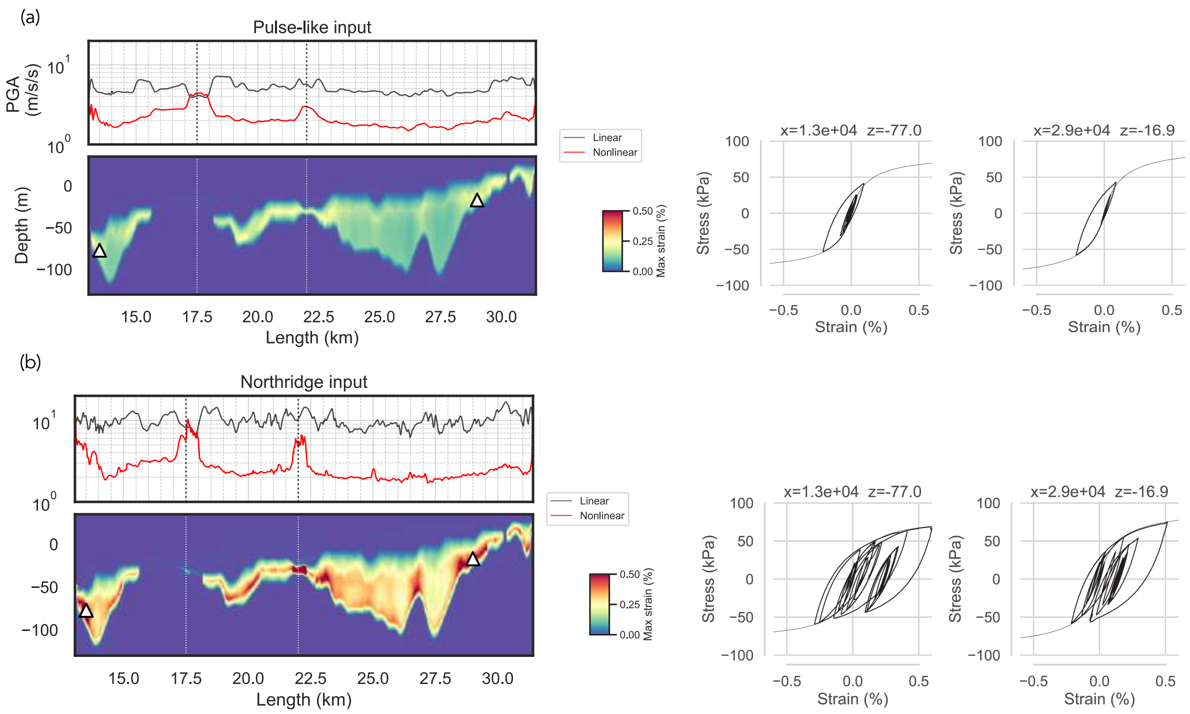

Figure 9. The effect of basin nonlinearity on peak ground motion for the two cases of input motion. (a) The comparison of PGA variation along the basin length between linear and nonlinear cases (top), and maximum strain distribution in the basin (bottom), and stress-strain curves at selected basin locations, for the case of Ricker input, (b) same as (a) for the case of Northridge input use. We only show the max. strain values for the nonlinear layer and set zero strain elsewhere in the 2D plots. Selected locations are denoted by triangles in the 2D plots. Wave incidence is vertical in both cases.

4 CONCLUSIONS

We found that the Kathmandu basin typically enhances low-frequency ground motion (< 2 Hz) with and without nonlinear soil behaviour, and regardless of wave incidence angle. This finding supports and expands the insights from past studies of ground motions produced by the 2015 Gorkha earthquake. Here, accounting for the 2D basin geometry, soil stratigraphy and multi-dimensional soil nonlinearity, thanks to the most recent geotechnical data, we find that low-frequency ground motion amplification in Kathmandu should be expected during future earthquakes.

We also found that the angle of wave incidence can tremendously boost the high-frequency ground motion across an entire basin, compared to bedrock, despite the damping effect of soil nonlinearity. In our models, ground motion amplification appears prominently (up to a factor of 5) at wave incidence angles larger than ∼42 degrees relative to vertical. We propose that

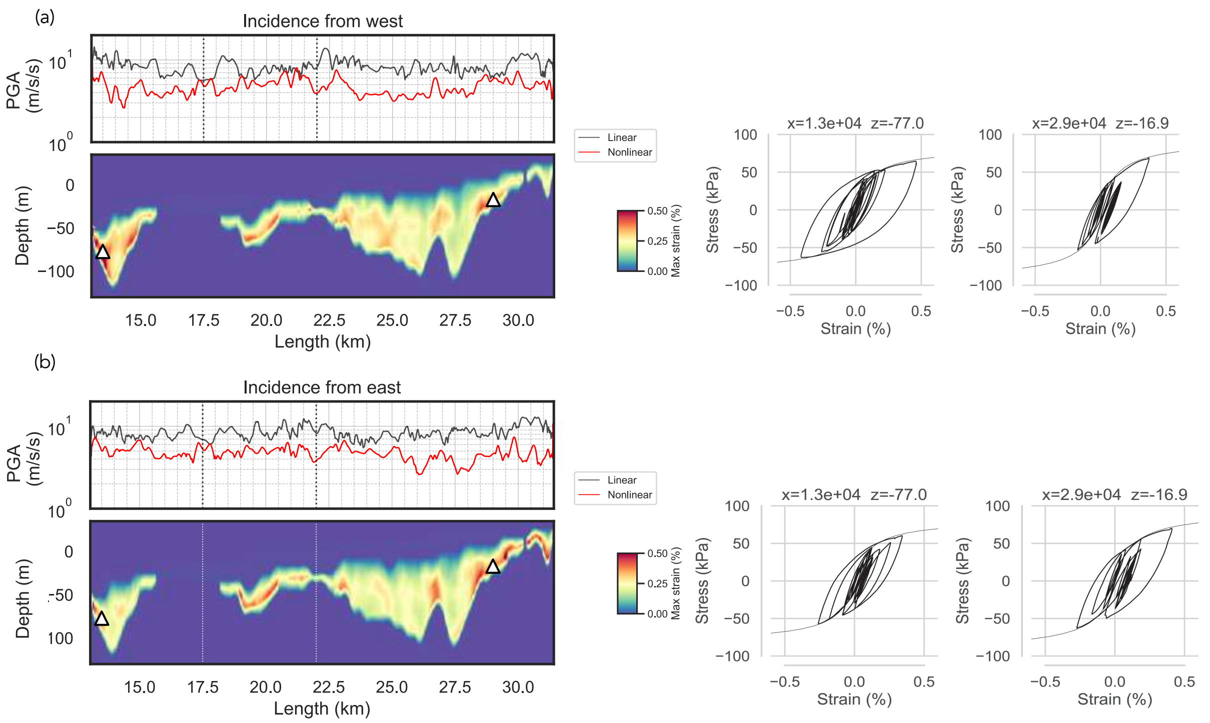

Figure 10. The effect of basin nonlinearity on peak ground motion for different wave incidence direction. (a) The comparison of PGA variation along the basin length between linear and nonlinear cases (top), and maximum strain distribution in the basin (bottom), and stress-strain curves at selected basin locations, for the case of wave incidence from west, (b) same as (a) for the case of wave incidence from east. We only show the max. strain values for the nonlinear layer and set zero strain elsewhere in the 2D plots. Selected locations are denoted by triangles in the 2D plots. The incidence angle equals 30 degrees in both cases.

the position of the source relative to the basin, through the effective wave incidence angle, may have contributed to the differences in damage impact between the Gorkha event and earlier earthquakes. Investigating in broadband to what extent such wave incidence effects prevail when considering 3D basin effects and finite sources can further advance seismic hazard studies in Kathmandu and other areas.

The spatial variability of ground motion along the Kathmandu basin can be enhanced by basin nonlinearity and wave incidence effects. Ground motion can be much stronger near basin edges compared to deeper parts of the basin (up to 5 times here) due to nonlinearity effects. The amplitude and location of amplification is also affected by the direction and angle of incident waves. While the significance of both soil nonlinearity and oblique wave incidence is well developed in the literature for simplified sites, our analyses on the Kathmandu basin highlight the necessity of considering their coupled effects in seismic hazard assessment studies worldwide on sites with complex basin geometry and soil stratigraphy, such as Los Angeles, Mexico City, and Grenoble basins. In that sense, further investigation on the above-mentioned factors can help to better constrain the spatial variability of ground motion in such areas.

ACKNOWLEDGEMENTS

This work was supported by the French National Research Agency (ANR) through project FAULTS_R_GEMS (grant ANR-17-CE31-0008) and Investments-in-the-Future project UCA-JEDI (grant ANR-15-IDEX-01).

Data and resources

All data needed to reproduce this work is available online: 2D wave propagation modelling tools can be found at https://github.com/jpampuero/sem2dpack. The updates can be followed in the same address.

REFERENCES

Ampuero, J.-P., 2012. A spectral element method tool for 2d wave propagation and earthquake source dynamics user's guide.

Ampuero, J.-P., Vilotte, J.-P., & Sanchez-Sesma, F., 2002. Nucleation of rupture under slip dependent friction law: simple models of fault zone, *Journal of Geophysical Research: Solid Earth*, **107**(B12), ESE–2.

Asimaki, D., Mohammadi, K., Mason, H. B., Adams, R. K., Rajaure, S., & Khadka, D., 2017. Observations and simulations of basin effects in the kathmandu valley during the 2015 gorkha, nepal, earthquake sequence, *Earthquake Spectra*, **33**(1_suppl), 35–53.

Auden, J. & Ghosh, A., 1935. Preliminary account of the earthquake of the 15th january, 1934, in bihar and nepal, *Records of the Geological Survey of India*, **68**(2), 177–239.

Avouac, J.-P., Meng, L., Wei, S., Wang, T., & Ampuero, J.-P., 2015. Lower edge of locked main himalayan thrust unzipped by the 2015 gorkha earthquake, *Nature Geoscience*, **8**(9), 708–711.

Ayoubi, P., Asimaki, D., & Mohammdi, K., 2018. Basin effects in strong ground motion: A case study from the 2015 gorkha, nepal, earthquake, in *Geotechnical earthquake engineering and soil dynamics V: Seismic hazard analysis, earthquake ground motions, and regional-scale assessment*, pp. 288–296, American Society of Civil Engineers Reston, VA.

Bonilla, L. F., Gélis, C., & Régnier, J., 2011. The challenge of nonlinear site response: Field data observations and numerical simulations, in *Proc. of Effects of Surface Geology on Seismic Motion, August 23-26, 2011*, University of California Santa Barbara.

Castro-Cruz, D., Regnier, J., Bertrand, E., & Courboulex, F., 2020. A new parameter to empirically describe and predict the non-linear seismic response of sites derived from the analysis of kik-net database, *Soil Dynamics and Earthquake Engineering*, **128**, 105833.

Chaljub, E., Komatitsch, D., Vilotte, J.-P., Capdeville, Y., Valette, B., & Festa, G., 2007. Spectral-element analysis in seismology, *Advances in geophysics*, **48**, 365–419.

Chen, G., Jin, D., Zhu, J., Shi, J., & Li, X., 2015. Nonlinear analysis on seismic site response of fuzhou basin, china, *Bulletin of the Seismological Society of America*, **105**(2A), 928–949.

Chen, M. & Wei, S., 2019. The 2015 gorkha, nepal, earthquake sequence: Ii. broadband simulation of ground motion in kathmanduthe 2015 gorkha, nepal, earthquake sequence: Ii. broadband simulation of ground motion, *Bulletin of the Seismological Society of America*, **109**(2), 672–687.

Chiaro, G., Kiyota, T., Pokhrel, R. M., Goda, K., Katagiri, T., & Sharma, K., 2015. Reconnaissance report on geotechnical and structural damage caused by the 2015 gorkha earthquake, nepal, *Soils and Foundations*, **55**(5), 1030–1043.

Clayton, R. & Engquist, B., 1977. Absorbing boundary conditions for acoustic and elastic wave equations, *Bulletin of the seismological society of America*, **67**(6), 1529–1540.

Dal Zilio, L., van Dinther, Y., Gerya, T., & Avouac, J.-P., 2019. Bimodal seismicity in the himalaya controlled by fault friction and geometry, *Nature communications*, **10**(1), 1–11.

De Luca, G., Marcucci, S., Milana, G., & Sano, T., 2005. Evidence of low-frequency amplification in the city of l'aquila, central italy, through a multidisciplinary approach including strong-and weak-motion data, ambient noise, and numerical modeling, *Bulletin of the Seismological Society of America*, **95**(4), 1469–1481.

Dixit, A. M., Yatabe, R., Dahal, R. K., & Bhandary, N. P., 2013. Initiatives for earthquake disaster risk management in the kathmandu valley, *Natural hazards*, **69**(1), 631–654.

Esmaeilzadeh, A., Motazedian, D., & Hunter, J., 2019. 3d nonlinear ground-motion simulation using a physics-based method for the kinburn basin, *Bulletin of the Seismological Society of America*, **109**(4), 1282–1311.

Frankel, A. D., Carver, D. L., & Williams, R. A., 2002. Nonlinear and linear site response and basin effects in seattle for the m 6.8 nisqually, washington, earthquake, *Bulletin of the Seismological Society of America*, **92**(6), 2090–2109.

Galetzka, J., Melgar, D., Genrich, J. F., Geng, J., Owen, S., Lindsey, E. O., Xu, X., Bock, Y., Avouac, J.-P., Adhikari, L. B., et al., 2015. Slip pulse and resonance of the kathmandu basin during the 2015 gorkha earthquake, nepal, *Science*, **349**(6252), 1091–1095.

Gélis, C. & Bonilla, L. F., 2012. 2-dp–sv numerical study of soil–source interaction in a non-linear basin, *Geophysical Journal International*, **191**(3), 1374–1390.

Gilder, C. E., Pokhrel, R. M., Vardanega, P. J., De Luca, F., De Risi, R., Werner, M. J., Asimaki, D., Maskey, P. N., & Sextos, A., 2020. The safer geodatabase for the kathmandu valley: Geotechnical and geological variability, *Earthquake Spectra*, **36**(3), 1549–1569.

Hashash, Y., Tiwari, B., Moss, R. E., Asimaki, D., Clahan, K. B., Kieffer, D. S., Dreger, D. S., Macdonald, A., Madugo, C. M., Mason, H. B., et al., 2015. Geotechnical field reconnaissance: Gorkha (nepal) earthquake of april 25, 2015 and related shaking sequence, *Geotechnical extreme event reconnaisance GEER association report No. GEER-040*, p. 1.

Hough, S. E. & Roger, B., 2008. Site response of the ganges basin inferred from re-evaluated macroseismic observations from the 1897 shillong, 1905 kangra, and 1934 nepal earthquakes, *Journal of Earth System Science*, **117**(2), 773–782.

Hough, S. E., Martin, S. S., Gahalaut, V., Joshi, A., Landes, M., & Bossu, R., 2016. A comparison of observed and predicted ground motions from the 2015 mw 7.8 gorkha, nepal, earthquake, *Natural Hazards*, **84**(3), 1661–1684.

Iwan, W. D., 1967. On a class of models for the yielding behavior of continuous and composite systems.

JICA, M., 2002. The study on earthquake disaster mitigation in the kathmandu valley, kingdom of nepal, *Japan International Cooperation Agency (JICA) and Ministry of Home Affairs (MOHA), Tokyo*.

Joyner, W. B., 1975. A method for calculating nonlinear seismic response in two dimensions, *Bulletin of the Seismological Society of America*, **65**(5), 1337–1357.

Kaushik, H., Bevington, J., Jaiswal, K., Lizundia, B., & Shrestha, S., 2016. Buildings (eeri earthquake reconnaissance team report: M7. 8 gorkha, nepal earthquake on april 25, 2015 and its aftershocks), Tech. rep., Earthquake Engineering Research Institute.

Komatitsch, D. & Vilotte, J.-P., 1998. The spectral element method: an efficient tool to simulate the seismic response of 2d and 3d geological structures, *Bulletin of the seismological society of America*, **88**(2), 368–392.

Laurendeau, A., Courboulex, F., Bonilla, L. F., Alvarado, A., Naya, V. A., Guéguen, P., Mercerat, E. D., Singaucho, J. C., Bertrand, E., Perrault, M., et al., 2017. Low-frequency seismic amplification in the quito basin (ecuador) revealed by accelerometric recordings of the renac networkamplification in the quito basin revealed by accelerometric recordings of the renac, *Bulletin of the Seismological Society of America*, **107**(6), 2917–2926.

Liu, S., Datta, S., Bouden, M., & Shah, A., 1991. Scattering of obliquely incident seismic waves by a cylindrical valley in a layered half-space, *Earthquake engineering & structural dynamics*, **20**(9), 859–870.

Marsh, J., Larkin, T., Haines, A., & Benites, R., 1995. Comparison of linear and nonlinear seismic responses of two-dimensional alluvial basins, *Bulletin of the Seismological Society of America*, **85**(3), 874–889.

Oral, E., Gélis, C., Bonilla, L. F., & Delavaud, E., 2017. Spectral element modelling of seismic wave propagation in visco-elastoplastic media including excess-pore pressure development, *Geophysical*

Journal International, **211**(3), 1494–1508.

Oral, E., Gélis, C., & Bonilla, L. F., 2019. 2-d p-sv and sh spectral element modelling of seismic wave propagation in non-linear media with pore-pressure effects, *Geophysical Journal International*, **217**(2), 1353–1365.

Papageorgiou, A. S. & Kim, J., 1993. Propagation and amplification of seismic waves in 2-d valleys excited by obliquely incident p-and sv-waves, *Earthquake engineering & structural dynamics*, **22**(2), 167–182.

Piya, B. K., 2004. Generation of a geological database for the liquefaction hazard assessment in kathmandu valley, *Master's Thesis*.

Psarropoulos, P., Tazoh, T., Gazetas, G., & Apostolou, M., 2007. Linear and nonlinear valley amplification effects on seismic ground motion, *Soils and Foundations*, **47**(5), 857–871.

Ragozzino, E., 2014. Nonlinear seismic response in the western l'aquila basin (italy): Numerical fem simulations vs. ground motion records, *Engineering geology*, **174**, 46–60.

Rajaure, S., Asimaki, D., Thompson, E. M., Hough, S., Martin, S., Ampuero, J., Dhital, M., Inbal, A., Takai, N., Shigefuji, M., et al., 2017. Characterizing the kathmandu valley sediment response through strong motion recordings of the 2015 gorkha earthquake sequence, *Tectonophysics*, **714**, 146–157.

Roten, D., Olsen, K., Day, S., Cui, Y., & Fäh, D., 2014. Expected seismic shaking in los angeles reduced by san andreas fault zone plasticity, *Geophysical Research Letters*, **41**(8), 2769–2777.

Sakai, H., 2001. Stratigraphic division and sedimentary facies of the kathmndu basin group, central nepal, *Journal of Nepal Geological Society*, **25**(1), 19–32.

Sakai, H., Fuji, R., & Kuwahara, Y., 2002. Changes in the depositional system of the paleo-kathmandu lake caused by uplift of the nepal lesser himalayas, *Journal of Asian Earth Sciences*, **20**(1), 267–276.

Sapkota, S., Bollinger, L., Klinger, Y., Tapponnier, P., Gaudemer, Y., & Tiwari, D., 2013. Primary surface ruptures of the great himalayan earthquakes in 1934 and 1255, *Nature Geoscience*, **6**(1), 71–76.

Singh, D. & Gupta, H. K., 1980. Source dynamics of two great earthquakes of the indian subcontinent: The bihar-nepal earthquake of january 15, 1934 and the quetta earthquake of may 30, 1935, *Bulletin of the Seismological Society of America*, **70**(3), 757–773.

Takai, N., Shigefuji, M., Rajaure, S., Bijukchhen, S., Ichiyanagi, M., Dhital, M. R., & Sasatani, T., 2016. Strong ground motion in the kathmandu valley during the 2015 gorkha, nepal, earthquake, *Earth, Planets and Space*, **68**(1), 1–8.

Wei, S., Chen, M., Wang, X., Graves, R., Lindsey, E., Wang, T., Karakaş, Ç., & Helmberger, D., 2018. The 2015 gorkha (nepal) earthquake sequence: I. source modeling and deterministic 3d ground shaking, *Tectonophysics*, **722**, 447–461.

Zhang, H., Van Der Lee, S., & Ge, Z., 2016. Multiarray rupture imaging of the devastating 2015 gorkha, nepal, earthquake sequence, *Geophysical Research Letters*, **43**(2), 584–591.

Zhang, N., Gao, Y., & Pak, R. Y., 2017. Soil and topographic effects on ground motion of a surficially inhomogeneous semi-cylindrical canyon under oblique incident sh waves, *Soil Dynamics and Earthquake Engineering*, **95**, 17–28.

Zhu, C., Thambiratnam, D. P., & Zhang, J., 2016. Response of sedimentary basin to obliquely incident sh waves, *Bulletin of Earthquake Engineering*, **14**(3), 647–671.